Activation of CREB drives acinar cells to ductal reprogramming and promotes pancreatic cancer progression in animal models of alcoholic pancreatitis

Supriya Srinivasan[1*], Siddharth Mehra[1*], Sudhakar Jinka[1], Anna Bianchi[1], Samara Singh[1], Austin R. Dosch[1], Haleh Amirian[1], Varunkumar Krishnamoorthy[1], Iago De Castro Silva[1], Manan Patel[1], Edmond Worley III Box[1], Vanessa Garrido[1], Tulasigeri M. Totiger[1], Zhiqun Zhou[1], Yuguang Ban[2], Jashodeep Datta[1,3], Michael VanSaun[4], Nipun Merchant[1,3], and Nagaraj S. Nagathihalli[1,3]

[*]Authors share co-first authorship.

Author Affiliations: [1]Department of Surgery, [2]Department of Public Health Sciences, University of Miami Miller School of Medicine, Miami, Florida. [3]Sylvester Comprehensive Cancer Center, University of Miami, Miami, Florida. [4]Department of Cancer Biology, University of Kansas Medical Center, Kansas City, Kansas.

Running Title: CREB in pancreatic cancer progression

Keywords: cAMP response element binding protein 1 (CREB); acinar-to-ductal metaplasia (ADM); alcoholic chronic pancreatitis (ACP), pancreatic intraepithelial neoplasia (PanIN); pancreatic ductal adenocarcinoma (PDAC); pancreatic cancer.

Funding: This study was supported by the R01 CA262526 grant from the National Institutes of Health (NIH) National Cancer Institute (NCI) and the James Esther and King Biomedical Research Program of the Florida Department of Health (22K06), awarded to N.S. Nagathihalli. The Histopathology Core Service was conducted with the assistance of the Sylvester Comprehensive Cancer Center support grant, under the supervision of N. Nagathihalli. The research presented in this paper received financial support from the NCI of the NIH through Award Number P30 CA240139. The authors bear full responsibility for the content and the opinions expressed in this work, which may not necessarily reflect the official perspectives of the NIH.

Corresponding Author: Nagaraj Nagathihalli, Division of Surgical Oncology, Department of Surgery, University of Miami Miller School of Medicine, 1550 NW 10th Ave., FOX 140L, Miami, Florida 33136, Phone: 305-243-3502, E-mail: nnagathihalli@med.miami.edu

Conflict of Interest: The authors declare no potential conflicts of interest.

Abstract

BACKGROUND & AIMS: Alcoholic chronic pancreatitis (ACP) exacerbates pancreatic damage through acinar cell injury, fibroinflammation, and cyclic adenosine monophosphate response element binding protein 1 (CREB) activation, surpassing the damage by alcohol (A) alone or cerulein-induced CP. The molecular cooperativity between CREB and oncogenic *Kras*$^{G12D/+}$(*Kras**) in promoting pancreatic cancer progression within the context of ACP remains unclear.

METHODS: Experimental ACP induction was established in multiple mouse models, with euthanasia during the recovery stage to assess tumor latency. We established CREB deletion (*Creb*$^{fl/fl}$) in *Ptf1a*$^{CreERTM/+}$*;LSL-Kras*$^{G12D/+}$(*KC*) genetic mouse models (*KCC*$^{-/-}$). Pancreata from *Ptf1a*$^{CreERTM/+}$, *KC*, and *KCC*$^{-/-}$ mice were analyzed using western blotting, phosphokinase array, and quantitative PCR. Single-cell RNA sequencing was performed in ACP-induced *KC* mice. Lineage tracing of acinar cell explant cultures and analysis of tissue samples from human pancreatic diseases (CP and pancreatic ductal adenocarcinoma [PDAC]) were conducted.

RESULTS: ACP induction in *KC* mice impaired the pancreas' repair mechanism. Acinar cell-derived ductal lesions demonstrated prolonged hyperactivated CREB in acinar-to-ductal metaplasia (ADM)/pancreatic intraepithelial neoplasia (PanIN) lesions associated with pancreatitis and in PDAC. Persistent CREB activation reprogrammed acinar cells, increasing profibrotic inflammation. In ACP-induced models, acinar-specific *Creb* ablation reduced advanced PanIN lesions, hindered tumor progression, and improved acinar cell function. Pharmacological targeting of CREB significantly reduced the primary tumor burden in a PDAC mouse model with ACP.

CONCLUSIONS: Our findings demonstrate that CREB and *Kras** promote irreversible ADM, accelerating pancreatic cancer progression with ACP. Targeting CREB offers a promising strategy to address the clinical need for effective treatments for inflammation-driven pancreatic cancer.

Introduction

Alcoholic pancreatitis, both acute and chronic, poses a significant risk of developing pancreatic cancer.[1, 2] Prolonged alcohol abuse accounts for 60–90% of chronic pancreatitis (CP) cases.[3, 4] Continuous inflammation due to alcoholic CP (ACP) causes pancreatic atrophy and fibrosis within and around the pancreas.[5]

Chronic pancreatic inflammation frequently involves acinar cell homeostasis loss and ductal phenotype acquisition, termed acinar-to-ductal metaplasia (ADM). This adaptive physiological response to inflammation protects the pancreas from further damage.[6] Nevertheless, scientific experimental models consistently demonstrate that activating inflammation in pancreatic tissue harboring the oncogene *Kras*$^{G12D/+}$ (*Kras**) impedes its ability to regenerate and expedites[7-9] the development of neoplastic precursor lesions, including pancreatic intraepithelial neoplasia (PanIN), progressing rapidly toward invasive carcinoma.[10, 11] The cooperative mechanisms of *Kras** and chronic inflammation in ACP remain poorly understood.

Our previous study elucidated the activation of the phosphatidylinositol 3-kinase/protein kinase B/mammalian target of rapamycin (mTOR) signaling pathway, leading to cyclic adenosine monophosphate response element binding protein 1 (CREB) activation within the inflammatory milieu of the pancreas.[12] We have identified CREB hyperactivation associated with poor prognosis in patients with aggressive pancreatic cancer.

We reported persistent CREB activation in acinar cells transitioning toward a ductal phenotype in *Kras** mice post-ACP induction. In *KC* mice with ACP induction, more high-grade PanIN lesions and an increased fibroinflammatory response were observed, reducing tumor latency and accelerating pancreatic cancer progression. To enhance our findings' translational relevance, we demonstrated elevated phosphorylated CREB (pCREB) expression within the ADM/PanIn lesions in the pancreatic tissues of patients with CP, ACP, and pancreatic ductal adenocarcinoma (PDAC). *Creb* deletion in *KC* mice acinar cells treated with ACP reduced ADM reprogramming, hindering tumor growth and prolonging tumor latency. Pharmacological targeting of CREB using a selective CREB inhibitor (CREBi, 666-15) markedly reduced primary tumor burden in

ACP-associated PDAC tumors in a syngeneic orthotopic *Kras*$^{G12D/+,}$ *Trp53*$^{R172H/+}$ *Pdx1*^{Cre} (KPC) mouse model. These findings provide a comprehensive understanding of CREB's oncogenic role with *Kras** in accelerating pancreatic cancer progression through chronic inflammation. The strong clinical relevance of CREB expression in human pancreatic diseases, including pancreatitis and cancer, underscores its potential as a promising therapeutic target for aggressive pancreatic cancer.

Materials and Methods

Creb Deletion in a Genetically Engineered Ptf1a$^{CreERTM/+}$*;LSL-Kras*$^{G12D/+}$ *(KC) Mice Model*

Ptf1a$^{CreERTM/+}$ knock-in allele mice were obtained from Jackson Laboratory (Bar Harbor, ME; stock number: 019378)[14] and crossed with *LSL-Kras*$^{G12D/+}$ to generate acinar-specific *Kras*$^{G12D/+}$ mutant mice, referred to as *Ptf1a*$^{CreERTM/+}$*;LSL-Kras*$^{G12D/+}$ (*KC*) mice. To generate acinar-specific *Creb1* (*Creb*) knockout mice, *Ptf1a*$^{CreERTM/+}$*; Creb*$^{fl/fl}$ mice were crossed with *LSL-Kras*$^{G12D/+}$*; Creb*$^{fl/fl}$ mice to generate *Ptf1a*$^{CreERTM/+}$*;LSL-Kras*$^{G12D/+}$*; Creb*$^{fl/fl}$ (KCC$^{-/-}$) mice. The *Creb*$^{fl/fl}$ mice were obtained from Professor Eric Nestler (Cold Spring Harbor Laboratory, Cold Spring Harbor, NY 11724).[15] *Creb* was selectively excised from acinar cells in LSL-Kras$^{G12D/+}$ mice using inducible Cre recombinase, expressed from the pancreas-specific *Ptf1a*$^{CreERTM/+}$ promoter. Cre recombinase activity was induced in 6-week-old mice through daily tamoxifen administration (Sigma-Aldrich, cat. # T5648) for 6 consecutive days at a dose of 0.15 mg/g body weight, followed by a 1-week rest before starting the ACP induction phase.

Lineage Tracing in R26R^{EYFP} *Reporter Mice*

R26R^{EYFP} mice (obtained from Jackson Laboratory; stock number: 006148)[16] were used for lineage tracing. To precisely trace the lineage of recombined acinar cells, *Ptf1a*$^{CreERTM/+}$ mice containing the *R26R*^{EYFP} reporter were crossed with *LSL-Kras*$^{G12D/+}$ mice to generate *Ptf1a*$^{CreERTM/+}$*;LSL-Kras*$^{G12D/+}$*; R26R*^{EYFP}. These mice were subsequently bred with *Creb*$^{fl/fl}$ mice to produce *Ptf1a*$^{CreERTM/+}$*;LSL-Kras*$^{G12D/+}$*; R26R*^{EYFP}*; Creb*$^{fl/fl}$ (hereafter referred to as *KCYC*$^{-/-}$) mice.

Mouse Genotyping

Genotyping was conducted using the automated genotyping service provider, Transnetyx (Cordoba, TN, USA). Supplementary Table 1 presents the probe sequences used for genotyping analysis.

Animal Studies

Here, mice of both sexes weighing 20–25 g were used; they were housed in pathogen-free conditions under a 12-h light-dark diurnal cycle with a controlled temperature of 21°C–23°C and maintained on a standard rodent chow diet (Harlan Laboratories) before the experimental induction of the ACP protocol. The mice were euthanized upon the manifestation of signs of compromised health, including weight loss, accelerated respiration, hunched posture, piloerection, and reduced activity. All animal experiments were approved and performed in compliance with the regulations and ethical guidelines for experimental and animal studies of the Institutional Animal Care and Use Committee and the University of Miami (Miami, FL; Protocol Nos. 15-057, 15-099, 18-081, and 21-093).

Establishing ACP In Vivo

The experimental mice were pair-fed with alcohol for 14 weeks using a Lieber-DeCarli alcohol-based liquid diet (A) (BioServ Inc., cat. #F1259SP) containing 5% v/v ethanol, whereas the control mice received a standard control liquid diet (C) (BioServ Inc., cat. #F1259SP) using 28% carbohydrates instead of ethanol. During the final 4 weeks of alcohol exposure, CP was induced by administering cerulein solubilized in phosphate-buffered saline to achieve a concentration of 10 mg/mL (ACP induction period). This feeding regimen mimics the pancreatic damage from chronic alcohol use in humans.[12, 17, 18] Cerulein was intraperitoneally delivered at a dose of 50 µg/kg through hourly injections (six times daily, 3 days weekly) over 4 weeks. This combined effect of alcohol and cerulein was observed in the ACP group. The animals were euthanized humanely to harvest the blood and pancreas after ACP induction on days 3 and 21 (ACP

recovery period). Supplementary Table 2 presents a comprehensive overview of the treatment groups spanning both the induction and recovery phases.

Tumor Latency Period Estimation

In the context of genetically engineered murine models (GEMMs), the tumor latency period is the duration between tumor initiation or formation and the point at which these pancreatic tumors become grossly discernible during biweekly abdominal palpation examinations. Mice exhibiting noticeable signs of illness attributed to an increased tumor burden were euthanized. Subsequently, the pancreatic tissues were collected and subjected to hematoxylin and eosin (H&E) staining for pathological analysis.

Pancreatic Digestion for Single-Cell RNA Sequencing (scRNA-seq) and Library Generation

The mouse pancreatic tissue harvested from control *KC* and *KC* with ACP induction were mechanically dissociated to generate single-cell suspensions, as previously described.[19] Pancreatic fragments (1–2 mm) were immersed in 0.02% trypsin C-ethylenediamine tetra acetic acid 0.05% (Biological Industries) for 10 min at 37°C with agitation, then washed with 10% fetal calf serum/Dulbecco's Modified Eagle Medium. For the next dissociation step, the cells were washed with Hanks' balanced salt solution (HBSS) × 1 containing 1 mg/mL collagenase P, 0.2 mg/mL bovine serum albumin (BSA), and 0.1 mg/mL trypsin inhibitor. After 20–30 min incubation at 37°C with agitation, the samples were pipetted up and down, returned to 37°C, passed through a 70-mm nylon mesh (Corning #431751), and washed two times with 1×HBSS containing 4% BSA and 0.1 mg/mL DNase I. The samples were divided into two equal volumes, with one sample subjected to centrifugation and washed three times at 60 × *g* to isolate large cells containing acinar cells. Simultaneously, the second sample was centrifuged and washed three times at 300 × *g* to collect all cells. If red blood cells were abundant in the second sample, they were treated with red blood cell lysis buffer (Sigma-Aldrich). Live cells were isolated using a MACS Dead Cell Removal Kit (Miltenyi Biotech #130-090-101). Finally, the two samples were combined at a cell ratio of 30% and 70% from the 60 × *g* and 300 × *g* samples, respectively, and processed for scRNA-seq library preparation by the Oncogenomics-Shared

Resource Facility (University of Miami). Briefly, the cells were counted, and 10,000 cells were loaded per lane on 10× chromium microfluidic chips. Single-cell capture, barcoding, and library preparation were performed using the Chromium 85 Controller, Chromium Next GEM Single Cell 3' GEM, Library & Gel Bead Kit v3.1, and Chromium Next GEM Chip G kit (10× Genomics), with a cell recovery target of 100,000 cells as per manufacturer's guidelines. The cDNA and libraries were sequenced using an Illumina NovaSeq 6000. The Cell Ranger pipeline (version 7.0, 10× Genomics) transformed Illumina base call files into FASTQ files, aligned them to the GRCm38 reference genome, and generated a digital gene-cell count matrix through the Biostatistics and Bioinformatics Shared Resource facility (University of Miami). Subsequently, the count matrices were imported into R version 3.5.0 and analyzed using the R package Seurat version 4.0.13-15.

For additional details on the experimental methodology, please refer to the Supplementary Materials and Methods section.

Results

Establishing ACP in Ptf1a$^{CreERTM/+}$ Mice

An ACP induction experimental mouse model was established in *Ptf1a*$^{CreERTM/+}$ mice, as described previously.[12] The mice were sacrificed after 3 or 21 days (ACP recovery period) (Figure 1*A*). All experimental cohort mice exhibited weight gain, with the vehicle and alcohol (A) groups showing maximum increase. Stopping exogenous ACP induction restored mouse body weight (identical to the control) 21 days after ACP induction (Supplementary Figure 1*A*). Serum levels revealed an increased blood alcohol concentration with A or ACP induction (Supplementary Figure 1*B*). *Ptf1a*$^{CreERTM/+}$ mice with ACP induction demonstrated markedly reduced pancreatic weight (implying pancreatic injury) (Supplementary Figure 1*C*). ACP withdrawal completely restored pancreatic weight to its normal level after 21 days (Supplementary Figure 1*D*). Alcohol-treated mice showed elevated serum amylase levels. Mice with ACP induction exhibited the most substantial decline in serum amylase levels among the

control, A, and CP mice (Supplementary Figure 1*E*), suggesting maximum acinar injury. Histological assessment of mouse pancreas harvested post-ACP induction (at day 3 of recovery) revealed profound injuries to the pancreatic tissue architecture, including acinar cell loss, duct-like structures (CK-19^{+} positivity), activated pancreatic stellate cells (PSCs) displaying alpha-smooth muscle actin positivity, increased collagen deposition (Sirius Red), and leukocyte infiltration (CD45^{+} immune cells) compared with the control, A-, or CP-exposed mice (Figure 1*B* and Supplementary Figure 1*F*). Pancreatic injury in *Ptf1a*$^{CreERTM/+}$ mice completely reversed after discontinuing the exogenous ACP stimulus (21-day recovery period) (Figure 1*B*). No histologically detectable PanINs occurred (Figure 1*B* and Supplementary Figure 1*F*) in all mouse cohorts. Quantitative PCR (qPCR)-based transcriptional profiling of ACP-treated mouse pancreata demonstrated marked downregulation of genes implicated in acinar cell regulation and function (Supplementary Figure 2*A*).

Activation of (CREB) is a Hallmark of ADM in Response to ACP

H&E (Figure 1*C*) and co-immunofluorescence (I.F) (Figure 1*D*) staining for CK19 and amylase in ACP-treated *Ptf1a*$^{CreERTM/+}$ mice revealed transient duct-like cells within 3 days of ACP induction. By the end of the 21-day recovery period, these cells redifferentiated and repopulated the acinar compartment, demonstrating the reversibility of ADMs.

We conducted phosphokinase array profiling on *Ptf1a*$^{CreERTM/+}$ mice pancreata post-ACP induction. Our analysis revealed a significant mTOR and CREB upregulation, two of the most prominently upregulated effector kinases, compared with the control pancreatic lysates (Figure *1E* and Supplementary Figure *2B*). Our laboratory's prior research identified CREB as a key effector of oncogenic mutant *Kras s*ignaling, linked to poor overall survival in patients with pancreatic cancer. Here, we studied CREB's involvement in ADM reprogramming and ductal plasticity enhancement.Further validation using immunoblotting and co-I.F. staining analysis uncovered a significantly elevated pCREB expression in duct-like structures 3 days post-ACP recovery, compared with the controls. By day 21 of ACP recovery, pCREB expression returned to baseline levels (Figure 1*F* and *G*). These findings suggest that ACP induces pancreatic injury,

fosters a fibroinflammatory milieu, and enhances CREB activation. Notably, these changes reversed during the recovery period, reducing CREB activation to baseline.

ACP Induction Accelerates ADM Reprogramming to PanIN and Pancreatic Cancer in Kras^{G12D} Mutant Mice

To enhance the evidence of ACP-mediated acinar cell reprogramming toward the ductal phenotype, we used *KC* GEMM harboring mutant *Kras** and established ACP induction (described in Figure 1*A*). Mice receiving an alcohol-based diet showed higher blood alcohol concentrations than control mice (Supplementary Figure 3*A*). Inducing ACP in *KC* mice considerably increased relative pancreatic weight (Figure 2*A*), without significant sex-specific differences (Supplementary Figure 3*B*).

The pancreas in control *KC* mice exhibited well-structured acinar compartments and low-grade PanIN lesions (Figure 2*B* and *C*). ACP-induced *KC* mice showed a substantially higher presence of mucinous ductal lesions (low-grade PanINs) with fewer acinar cells (after a 3-day recovery period) than A- or CP-induced *KC* mouse pancreata (Figure 2*C* and Supplementary Figure 3*C* and *3D*). After ACP induction and 21-day recovery, pancreatic tissue histological analysis revealed these mucinous PanIN progressions toward high-grade lesions (Figure 2*B* and *C*) and a significant increase in CK-19^{+} ductal positivity, mucin content, activated PSCs, increased collagen deposition, and infiltration of CD45^{+} immune cells (Figure 2*B*). This increase was higher in the ACP experimental cohort of *KC* mice pancreata than in A- or CP mice (Supplementary Figure 3*C*). A substantial increase in the deposition of extracellular matrix and increased infiltration of immune cells accompanied this progression (Figure 2*B* and Supplementary Figure 3*C*). Chronic inflammatory stimuli from ACP induction caused a higher increase in pCREB activation, correlating with maximum pancreatic damage in this group than in the control, A, or CP alone (Supplementary Figure 3*E*).

scRNA-seq was performed on live single-cell suspensions of *KC* mice pancreata, either control or ACP. Overall, 7903 and 7797 cells from the control and ACP groups were analyzed, respectively. UMAP cell clusters were annotated by examining classic cell type markers.[19, 20] We

distinguished nine distinct clusters representing different cell types (Figure 2*D* and Supplementary Figure 3*F*). ACP-induced *KC* mice exhibited an increased abundance of cell types, including ductal cells, macrophages, neutrophils, regulatory T cells, and fibroblasts, compared with the control mice (Figure 2*E*). Transcriptional analysis of the acinar cell compartment of *KC* mice pancreas showed upregulation of mRNA transcripts related to inflammation-induced stress, growth, and proliferation with ACP induction compared with the control mice (Figure 2*F*). Gene Ontology Biological Process (GOBP) analysis revealed that genes in the acinar subcluster exhibited differential expression related to cellular stress, apoptosis, alcohol metabolism response, and epithelial cell differentiation, consistent with ACP induction in *KC* GEMM mice (Figure 2*G*). The uninjured control *KC* pancreata showed more amylase$^+$ acinar cells with CK19$^+$ expression associated with the ductal structures, as revealed using co-I.F. analysis (Figure 2*H*). In ACP-treated *KC* mice, the acinar compartment progressively transformed and was replaced by a substantial proportion of ductal structures of acinar origin (dual CK19$^+$amylase$^+$ cells) after 3 days of recovery. Pancreatic tissue analysis at the end of the 21-day recovery period revealed a ductal phenotype with the highest proportion of CK19$^+$ cells (Figure 2*H*).

qPCR validation of transcriptional alterations in ACP-induced *KC* mice pancreata confirmed the reprogramming of acinar cells toward ductal metaplasia (Figure 2*I*). Advanced-grade histological lesions progressing to pathologically evident cancer in *KC* mice' pancreata with ACP induction correlated with a significantly shortened tumor latency period (Figure 2*J*, mean=5.80 months) compared with control (mean=9.76 months), A (mean=8.67 months), or CP (mean=7.56 months)-exposed *KC* mice, confirming a higher tumor burden induced by ACP than damage from A or CP induction alone.

CREB is Persistently Activated During PanIN Progression in Kras^{G12D} Mutant Mice and in Human CP

Histological assessment using co-I.F. analysis of pancreatic tissues harvested post-ACP induction in *KC* mice substantially increased pCREB-positive staining within CK19$^+$ ducts during the ACP recovery periods (3 and 21 days) compared with the control pancreata (Figure

3*A*). Western blotting (Figure 3*B*) confirmed heightened and sustained CREB activation in ACP-induced *KC* mice at 3, 21, and 42 days post-ACP recovery, suggesting a positive feed-forward loop in oncogenic *Kras* in driving CREB expression.

We combined the acinar-targeted *KC* GEMM with *R26R-EYFP* to generate the *Ptf1a-*$^{CreERTM/+}$*;LSL-Kras*$^{G12D/+}$*;R26R-EYFP (KCY)* mouse model (Figure 3*C*). The *KCY* mice underwent ACP induction (Figure 1*A*). Tamoxifen administration to *KCY* mice achieved approximately 95% recombination efficiency in acinar cells for 24 h.[14] In control *KCY* mice, YFP expression was mainly in acinar cells and excluded from CK19^{+} ducts. ACP-induced pancreatic injury in *KCY* mice accelerated PanIN progression (similar to *KC*-ACP), with many ductal structures originating from acinar cells (YFP^{+}CK19^{+}ducts) (Figure 3*C*). We observed sustained CREB activation within acinar-derived YFP/CK-19 dual-positive ductal lesions at 3- and 21-day recovery periods post-ACP induction. These results suggest CREB's role in reprogramming acinar cells into preneoplastic precursors with ACP (Figure 3*D*).

To further evaluate CREB localization and expression patterns in human pancreatic diseases, we analyzed its expression using immunohistochemistry (IHC) in the pancreata of patients with CP and those with a history of chronic alcohol consumption. Among the 72 analyzed pancreatic tissue cores, 43 (60%) showed high pCREB expression within the ADM regions affiliated with CP compared with the normal pancreas. Strong pCREB expression was additionally observed within the ADM lesions of pancreatitis in patients with a history of alcohol consumption as well (Figure 3*E*).

Acinar-specific Ablation of CREB Attenuates SpontaneousKras^{G12D}*-mediated PanIN Progression*

We generated acinar-specific conditional *Creb* knockout mice with *Kras** (Figure 4*A*) (*Ptf1a*$^{CreERTM/+}$*; LSL-Kras*$^{G12D/+}$*; Creb*$^{fl/fl}$ or *KCC*$^{-/-}$), whereas *KC* mice with wild-type *Creb* were called *KC*. The pancreata were collected from these two mouse cohorts at 5 and 10 months of age. The relative pancreatic weight of *KC* mice with *Creb* deletion (*KCC*$^{-/-}$) markedly reduced compared with that of wild-type *KC* mice (Figure 4*B* and *C*). Histological examination showed that the pancreata of 5-month-old *KC* mice displayed a higher prevalence of ADM and low-grade

PanIN lesions (Figure 4*D* and *E*), whereas that of 5-month-old *KCC*$^{-/-}$ mice showed no precursor lesions and demonstrated a normal architecture. Pancreata harvested from 10-month-old *KCC*$^{-/-}$ mice displayed infrequent ADM or PanIN1 lesions. Conversely, 10-month-old *KC* mice pancreata exhibited marked high-grade PanIN lesions and cancer (Figure 4*D* and *E*).
Co-I.F. analysis in *KC* and *KCC*$^{-/-}$ mice (10 months old) confirmed a significant reduction in pCREB expression in the pancreas' ductal regions in *KCC*$^{-/-}$ mice (Figure 4*F*). Pancreatic acinar cells were isolated from *KC* and *KCC*$^{-/-}$ mouse pancreata for explant culture. Acinar-specific *Creb* ablation significantly blocked ductal-like structure formation compared with acinar cells with intact CREB (Figure 4*G*). qPCR analysis of 10-month-old *KCC*$^{-/-}$ mice pancreata revealed reduced ductal cell phenotype genes, with a concomitant upregulation in genes linked to acinar cell regulation, function, proliferation, and differentiation compared with wild-type *KC* (Figure 4*H*). These results indicate that CREB ablation reduces acinar cells' ability to undergo ADM reprogramming.

Acinar-specific Ablation of Creb Attenuates Kras-mediated PanINs to Pancreatic Cancer Progression with ACP*

In *Ptf1a*$^{CreERTM/+}$ mice with *Creb* deletion (CC$^{-/-}$) without *Kras** (Supplementary Figure 4*A*), histological assessment confirmed the loss of CREB expression within *Ptf1a*$^{CreERTM/+}$*;Creb*$^{fl/fl}$ (CC$^{-/-}$) mice pancreata compared with wild-type *Ptf1a*$^{CreERTM/+}$ (C) mice (Supplementary Figure 4*B*). *Creb*-deleted mice exhibited enhanced acinar cell regenerative potential post-ACP induction (Supplementary Figure 4*C*). The improved recovery in *CC*$^{-/-}$ mice was associated with reduced CK19^{+} ducts and attenuated fibroinflammatory milieu.

To assess acinar-specific *Creb* ablation's capacity to counteract *Kras**-driven ADM/PanIN originating from the acini, we histologically compared *KC* and *KCC*$^{-/-}$ mouse pancreata (both at 3- and 21-day recovery). *KC* and *KCC*$^{-/-}$ mice maintained on a standard liquid diet were used as controls (Figure 5*A*). ACP induction in *KC* mice considerably increased the relative pancreatic weight (21-day recovery period), confirming a higher tumor burden than that in the control *KC* mice (Supplementary Figure 5*A*). This was less prominent in *KCC*$^{-/-}$ mice with ACP induction,

where CREB was deleted (Supplementary Figure 5*A* and *B)*, suggesting an association between attenuated tumor burden and CREB loss.

Creb genetic depletion in *KCC*$^{-/-}$ mice pancreata remarkably protected against ACP-triggered ADM and PanIN progression as evidenced by H&E, CK19, and Alcian blue staining (Figure 5*A* and *B*). Post-ACP induction, *KC* mice pancreata displayed a higher prevalence of high-grade PanIN lesions along with pancreatic cancer. Conversely, *KCC*$^{-/-}$ mice pancreatic tissue architecture displayed mostly normal organization of acinar cells, with fewer ADMs and low-grade PanIN lesions (Figure 5*A* and *B*). A notable reduction in the fibroinflammatory milieu (Sirius red and CD45^{+} cells) was observed (3- and 21-day ACP recovery periods) compared with that in *KC* GEMM. Similar beneficial histological trends occurred in control *KCC*$^{-/-}$ mice. Co-I.F. staining within *KC* and *KCC*$^{-/-}$ mice pancreatic tissues showed a notably heightened proportion of amylase-positive acinar cells in *Creb*-depleted KCC$^{-/-}$ mice (Figure 5*C*). Conversely, *KC* mice pancreata exhibited substantial damage resulting from ACP induction, with high CK-19^{+} cell abundance and loss of amylase^{+} acini.

Acinar-specific Ablation of CREB Attenuates ACP-Induced Acinar Cells to Ductal Reprogramming and Increases Tumor Latency Period

We studied ACP-induced pancreatic injury in a lineage tracing mouse model of *KC (KCY; Ptf1a-CreERTM/+;LSL-Kras*$^{G12D/+}$*;R26R-EYFP)* and *KCYC*$^{-/-}$ (*Creb* deletion in *KCY)* mice (Figure 6*A*). Co-I.F. staining displayed more YFP^{+}/CK19^{+} ductal lesions concurrent with the loss of the acinar cell compartment upon ACP induction in *KCY* mice. We found a substantial reduction in ductal structures, with minimal cells exhibiting dual positivity of YFP^{+}/CK19^{+} during ACP-induced *KCYC*$^{-/-}$. qPCR analysis confirmed a notable decrease in the mRNA expression levels of genes associated with ductal cell identity and function (*Sox9*, *Krt19*, *Aldh1a3*, and *Tspan8*) in ACP-treated *KCC*$^{-/-}$ mice pancreata compared with *KC* mice (Figure 6*B*).

Creb-deficient GEMMs (*KCC*$^{-/-}$ and *KCYC*$^{-/-}$*)* displayed low-grade PanIN lesions and a diminished pancreatic ductal phenotype, further reflected in tumor latency. ACP-induced *KCC*$^{-/-}$ mice pancreata had a mean pathological malignancy duration of 14.48 months (Figure 6*C*) compared with 5.80 months for *KC*-ACP mice. Conversely, control *KC* harboring wild-type

Creb and *KCC*$^{-/-}$ exhibited greater tumor latency (9.76 vs. 19 months) (Figure 6*C*). Overall, these results suggest that acinar-specific *Creb* ablation reduces ACP-induced acinar-to-ductal reprogramming and *Kras**-induced neoplastic progression, delaying tumor burden (Figure 6*D*).

Elevated CREB Expression in Human PDAC and Its Pharmacological Targeting in ACP *with PDAC Tumorigenesis*

We procured archived pancreatic tissue samples from patients who underwent curative surgical resection at the University of Miami (Figure 6*E*). IHC-based qualitative assessment of these patients revealed increased pCREB levels within ADM/PanIN lesions of severe pancreatitis and ductal adenocarcinoma compared with the normal pancreas (Figure 6E). In patients with PDAC, TMA analysis revealed substantially elevated pCREB expression in ADM/PanIN epithelial cell lesions compared with morphologically normal pancreatic acinar and ductal cells (Figure *6F*). *CREB* mRNA expression exponentially increased across different stages of PDAC in the ICGC patient cohort (Supplementary Figure *6A*), suggesting a strong correlation between CREB expression and disease progression in the regions of pancreatitis and pancreatic cancer.

We investigated whether CREB could be pharmacologically targeted to inhibit cancer progression in PDAC with or without ACP. We generated a KPC syngeneic orthotopic mouse model using C57/BL6 mice. The mice were maintained on an ACP diet and treated with a specific CREB inhibitor (CREBi: 666-15, 20 mg/kg) for 3 weeks (Figure *6G*). Pharmacological CREB inhibition markedly reduced the primary tumor burden in KPC orthotopic tumor-bearing mice with ACP induction compared with that in control or vehicle-treated mice, underscoring CREB's potential as a novel therapeutic target in PDAC with ACP.

We identified CREB's direct downstream targets that could be involved in ADM reprogramming-mediated cancer progression. Thus, we performed ChIP-seq analysis after CREB pulldown in KPC mouse tumor cells to identify CREB downstream targets (Supplementary Figure 6*B)*. Our findings revealed that CREB binds significantly to the *Srsf1* promoter region, a splicing factor that promotes pancreatitis and *Kras**-mediated PDAC initiation and progression[21] (Supplementary Figure 6*C*). Heightened SRSF1 expression occurred in ADM/PanIN lesions of

severe pancreatitis and ductal adenocarcinoma compared with normal pancreatic regions (Supplementary Figure 6*D)*. A significant correlation was observed between *CREB* and *SRSF1* mRNA expression in the Cancer Genome Atlas cohort of patients with PDAC (Supplementary Figure 6*E)*, with validation of their colocalization within the ductal epithelium of human PDAC tissue specimen via RNA fluorescence *in situ* hybridization co-I.F. analysis (Supplementary Figure 6*F)*. IHC-based histological profiling of *KC* and $KCC^{-/-}$ mice pancreata revealed increased SRSF1 expression within ADM/PanIN lesions, correlating with CREB activation in *KC* mice with ACP induction (Supplementary Figure 6*G*). Conversely, CREB-deleted mice pancreata displayed significantly attenuated SRSF1 expression (with and without ACP), confirming CREB's role in regulating SRSF1 in GEMM models of PDAC Overall, these results suggest that CREB-mediated transcriptional regulation of *Srsf1* is a potential direct downstream mediator of pancreatic cancer progression along with *Kras** and ACP.

Discussion

Pancreatic cancer, also called PDAC, is a fatal disease characterized by widespread genomic alterations and extensive tumor cell heterogeneity.[22-24] Previous studies in mouse models have highlighted that both acinar and ductal cells can result in PDAC, with acinar cells more amenable to display cellular plasticity and transform into a progenitor-like cell type with ductal characteristics (ADM), driving neoplastic progression with chronic inflammation or *Kras**.[6, 8, 11, 25] Consistent with previous studies, our findings demonstrate ADM reversible adaptability and reduced fibroinflammatory milieu in $Ptf1a^{CreERTM/+}$ mice without *Kras** irrespective of mouse sex.[26] Chronic inflammatory stimulation of ACP with *Kras** drives irreversible acinar cell transdifferentiation toward ADM, advancing PanINs and accelerating pancreatic cancer progression. An unbiased phosphokinase screening array revealed sustained hyperactivation of intrinsic CREB in acinar cells as a key oncogenic transcription factor, cooperating with *Kras** to drive this cellular transformation toward cancer (Figure 7).

This study investigated ACP development in mouse models using alcohol and supraphysiological doses of cerulein. The most ACP mouse models' noticeable feature reported

here was their ability to closely mimic human disease's features[12, 27-32], leading to profound damage within the pancreas and affecting its subcellular tumor immune and stromal components more severely than alcohol or CP alone. Our findings indicate that ACP induces heightened CREB activation, which is not observed to the same extent in non-ACP models. Our scRNA-seq analysis of *KC*-ACP GEMM revealed acinar cell populations enriched in pathways prominently related to cellular responses to stress and reactive oxygen species (ROS). Simultaneously, we observed a profound accumulation of innate immunosuppressive myeloid subsets–macrophages and granulocytes within ACP-exposed *KC* mice pancreata compared with the control. A recent study has highlighted oxidative stress-mediated crosstalk's role between acinar and macrophage populations in driving irreversible ADM–PanIN progression alongside fibrotic stroma generation within the lesion microenvironment as a tumor development foundation.[33] Here, we hypothesized that with experimentally induced ACP and *Kras**, this stress-mediated acinar macrophage interaction intensifies CREB activation compared with alcohol or CP alone. However, this hypothesis warrants further exploration in subsequent studies using the *KC* GEMM.

Since chronic inflammation is associated with pancreatic cancer, our study demonstrates CREB expression' critical role and localization in human pancreatic diseases' progression within alcohol-affiliated CP and ductal adenocarcinoma. Elevated pCREB expression in the ADM/PanIN lesions of CP and cancer, compared with the normal pancreas regions, suggests that CREB activation is an early and potentially critical event in disease progression. TMA and publicly available PDAC datasets confirmed its overexpression in this tumor type. These findings align closely with those of Srinivasan et al. study, demonstrating that CREB overexpression was associated with poor survival outcomes in patients with PDAC.[13] Our study bridges the gap between the findings observed in GEMM with chronic inflammation and human pancreatic diseases and establishes CREB as a pivotal oncogenic transcription factor.

These findings extensively characterized CREB-deleted GEMMs with *Kras**. Acinar-specific CREB loss significantly attenuated both spontaneous and ACP-mediated ADM/PanIN formation while simultaneously promoting acinar cells' regeneration in *KC* GEMM. Pharmacological targeting of CREB with a specific small molecule inhibitor decreased tumor growth with ACP.

Pancreatic cancer cell heterogeneity is mainly governed by exocrine compartment plasticity. Acinar cell transition to a duct-like identity makes them susceptible to *Kras**-induced precancerous lesions. Multiple factors and downstream signaling pathways mediate *Kras** induced cell transformation and tumorigenesis. Here, we used ChIP-seq to reveal the mechanisms of the proposed CREB actions in ADM and PanIN progression. Among CREB's direct downstream mediators identified, we noted significant binding to the *SRSF1* promoter, a splicing factor overexpressed in pancreatitis and pancreatic cancer. *SRSF1,* implicated in *Kras*^{G12D}-mediated PDAC initiation and progression, shows elevated expression correlating with poor survival outcomes.[21]

Recent studies have established additional mechanisms of chronic inflammation driving ADM/PanIN progression by activating ROS-mediated epidermal growth factor (EGF)-EGF receptor (EGFR) signaling pathways through epithelial-myeloid crosstalk.[33] One of the prerequisites for SRSF1-mediated PDAC initiation and progression is activating mitogen-activated protein kinase (MAPK) signaling. This study did not explore the crosstalk between EGFR–MAPK and CREB or CREB-regulated factors, including SRSF1. Future studies should explore CREB as a regulator of this cellular crosstalk to investigate immune cell dynamics.

In conclusion, ACP induction promotes pancreatic cancer progression via irreversible ADM reprogramming with *Kras** cooperativity. These ductal lesions originating from acinar cells display continuous CREB hyperactivation. Attenuating high-grade PanIN formation and tumor progression through acinar-specific loss of *Creb* provide foundational insights for future studies on CREB's role in pancreatic cancer progression in the ACP with *Kras**.

Acknowledgements

The authors thank Dr. Erin Dickey for her assistance in the editing process and Dr. Oliver McDonald for his help in assessing the histopathology sections. Research reported in this publication was performed in part at the Analytical Imaging Shared Resource (AISR), Onco-Genomics Shared Resource (OGSR;RRID:SCR_022502), Cancer Modeling Shared Resource (CMSR;RRID:SCR_022891), and Biostatistics and Bioinformatics Shared Resource (BBSR;RRID:SCR_022890) of the Sylvester Comprehensive Cancer Center at the University of Miami Miller School of Medicine, which is supported by the National Cancer Institute Cancer Center Support Grant (CCSG) P30-CA240139. BioRender was used for the creation of Figure 4A (License agreement SC265R8O4S) and Supplementary Figure 4*A* (License agreement RS265R8Z28).

Abbreviations

ADM; acinar to ductal metaplasia, ACP; alcoholic chronic pancreatitis, CK-19; cytokeratin 19, CP; chronic pancreatitis, CREB; cyclic AMP response element binding protein 1, EYFP; enhanced yellow fluorescent protein, GEMM; genetically engineered mouse model, I.F; Immunofluorescence, KC; Ptf1a$^{CreERTM/+}$;LSL-Kras$^{G12D/+}$, KCC$^{-/-}$; Ptf1a$^{CreERTM/+}$;LSL-Kras$^{G12D/+}$ Creb$^{floxed/floxed}$, PanIN; pancreatic intraepithelial neoplasia, PSCs; pancreatic stellate cells, scRNAseq; single-cell RNA sequencing, αSMA; α smooth muscle actin, TME: tumor microenvironment, UMAP: uniform manifold approximation and projection for dimension reduction.

Data Availability

Single cell RNA sequencing data are available at the Sequence Read Archive of NCBI under the BioProject ID: PRJNA109588

References

1. Peery AF, Crockett SD, Murphy CC, et al. Burden and cost of gastrointestinal, liver, and pancreatic diseases in the United States: update 2021. Gastroenterology 2022;162:621-44.
2. Nieto LM, Salazar M, Kinnucan J, et al. Incidence, burden, and predictors of readmission for acute alcoholic pancreatitis: a national analysis over 11 months. Dig Dis Sci 2023;68:423-33.
3. Singer MV. Effect of ethanol and alcoholic beverages on the gastrointestinal tract in humans. Rom J Gastroenterol 2002;11:197-204.
4. Dufour MC, Adamson MD. The epidemiology of alcohol-induced pancreatitis. Pancreas 2003;27:286-90.
5. Yadav D, Lowenfels AB. The epidemiology of pancreatitis and pancreatic cancer. Gastroenterology 2013;144:1252-61.
6. Strobel O, Dor Y, Alsina J, et al. In vivo lineage tracing defines the role of acinar-to-ductal transdifferentiation in inflammatory ductal metaplasia. Gastroenterology 2007;133:1999-2009.
7. Morris JPt, Cano DA, Sekine S, et al. Beta-catenin blocks Kras-dependent reprogramming of acini into pancreatic cancer precursor lesions in mice. J Clin Invest 2010;120:508-20.
8. Kopp JL, von Figura G, Mayes E, et al. Identification of Sox9-dependent acinar-to-ductal reprogramming as the principal mechanism for initiation of pancreatic ductal adenocarcinoma. Cancer Cell 2012;22:737-50.
9. Storz P. Acinar cell plasticity and development of pancreatic ductal adenocarcinoma. Nat Rev Gastroenterol Hepatol 2017;14:296-304.
10. Storz P, Crawford HC. Carcinogenesis of pancreatic ductal adenocarcinoma. Gastroenterology 2020;158:2072-81.

11. Asahina K, Balog S, Hwang E, et al. Moderate alcohol intake promotes pancreatic ductal adenocarcinoma development in mice expressing oncogenic Kras. Am J Physiol Gastrointest Liver Physiol 2020;318:G265-76.
12. Mehra S, Srinivasan S, Singh S, et al. Urolithin A attenuates severity of chronic pancreatitis associated with continued alcohol intake by inhibiting PI3K/AKT/mTOR signaling. Am J Physiol Gastrointest Liver Physiol 2022;323:G375-86.
13. Srinivasan S, Totiger T, Shi C, et al. Tobacco carcinogen-induced production of GM-CSF activates CREB to promote pancreatic cancer. Cancer Res 2018;78:6146-58.
14. Kopinke D, Brailsford M, Pan FC, et al. Ongoing Notch signaling maintains phenotypic fidelity in the adult exocrine pancreas. Dev Biol 2012;362:57-64.
15. Covington HE 3rd, Maze I, Sun H, et al. A role for repressive histone methylation in cocaine-induced vulnerability to stress. Neuron 2011;71:656-70.
16. DelGiorno KE, Hall JC, Takeuchi KK, et al. Identification and manipulation of biliary metaplasia in pancreatic tumors. Gastroenterology 2014;146:233-44.
17. Perides G, Tao X, West N, et al. A mouse model of ethanol dependent pancreatic fibrosis. Gut 2005;54:1461-7.
18. D'Souza El-Guindy NB, Kovacs EJ, De Witte P, et al. Laboratory models available to study alcohol-induced organ damage and immune variations: choosing the appropriate model. Alcohol Clin Exp Res 2010;34:1489-511.
19. Schlesinger Y, Yosefov-Levi O, Kolodkin-Gal D, et al. Single-cell transcriptomes of pancreatic preinvasive lesions and cancer reveal acinar metaplastic cells' heterogeneity. Nat Commun 2020;11:4516.
20. Hosein AN, Huang H, Wang Z, et al. Cellular heterogeneity during mouse pancreatic ductal adenocarcinoma progression at single-cell resolution. JCI Insight 2019;5:e129212
21. Wan L, Lin K-T, Rahman MA, et al. Splicing factor SRSF1 promotes pancreatitis and KRASG12D-mediated pancreatic cancer. Cancer Discov 2023;13:1678-95.
22. Aung KL, Fischer SE, Denroche RE, et al. Genomics-driven precision medicine for advanced pancreatic cancer: early results from the COMPASS trial. Clin Cancer Res 2018;24:1344-54.

23. Werba G, Weissinger D, Kawaler EA, et al. Single-cell RNA sequencing reveals the effects of chemotherapy on human pancreatic adenocarcinoma and its tumor microenvironment. Nat Commun 2023;14:797.
24. O'Kane GM, Grünwald BT, Jang G-H, et al. GATA6 expression distinguishes classical and basal-like subtypes in advanced pancreatic cancer. Clin Cancer Res 2020;26:4901-10.
25. Habbe N, Shi G, Meguid RA, et al. Spontaneous induction of murine pancreatic intraepithelial neoplasia (mPanIN) by acinar cell targeting of oncogenic Kras in adult mice. Proc Natl Acad Sci U S A 2008;105:18913-8.
26. Obafemi TF, Yu P, Li J, et al. Comparable responses in male and female mice to cerulein-induced chronic pancreatic injury and recovery. JOP 2018;19:236-43.
27. Vonlaufen A, Phillips PA, Xu Z, et al. Withdrawal of alcohol promotes regression while continued alcohol intake promotes persistence of LPS-induced pancreatic injury in alcohol-fed rats. Gut 2011;60:238-46.
28. Lugea A, Tischler D, Nguyen J, et al. Adaptive unfolded protein response attenuates alcohol-induced pancreatic damage. Gastroenterology 2011;140:987-97.
29. Xu S, Chheda C, Ouhaddi Y, et al. Characterization of mouse models of early pancreatic lesions induced by alcohol and chronic pancreatitis. Pancreas 2015;44:882-7.
30. Dawra R, Sah RP, Dudeja V, et al. Intra-acinar trypsinogen activation mediates early stages of pancreatic injury but not inflammation in mice with acute pancreatitis. Gastroenterology 2011;141:2210-7.
31. Sah RP, Dudeja V, Dawra RK, et al. Cerulein-induced chronic pancreatitis does not require intra-acinar activation of trypsinogen in mice. Gastroenterology 2013;144:1076-85.
32. Tao J, Cheema H, Kesh K, et al. Chronic pancreatitis in a caerulein-induced mouse model is associated with an altered gut microbiome. Pancreatology 2022;22:30-42.
33. Döppler HR, Storz P. Macrophage-induced reactive oxygen species in the initiation of pancreatic cancer: a mini-review. Front Immunol 2024;15:1278807.

Figure Legends

Figure 1. CREB activation in alcoholic chronic pancreatitis (ACP) in *Ptf1a*$^{CreERTM/+}$ mice. (A) ACP induction in *Ptf1a*$^{CreERTM/+}$ mice exposed to ethanol (alcohol)-enriched liquid diet (A) and caerulein administration (CP). Mice were euthanized after 3- and 21-day recovery periods. (B) Mouse pancreas with H&E and quantification depicting ducts (CK19^{+}), PanINs (Alcian Blue), collagen (Sirius red), and immune cells (CD45^{+}) (n=5 mice per group). (C) H&E-based quantification of mice pancreata highlighting acinar and ADM regions (n=3 mice per group). (D) Representative images of pancreas depicting amylase (green)/CK19 (red) co-I.F labeling and CK19^{+} amylase^{+} cell corresponding quantification (n=3 mice per group). (E) Mouse kinase array in control (ctrl) and ACP-induced pancreata. (F) Western blotting showing pCREB in pancreatic tissue lysates in ctrl, 3- and 21-day ACP recovery period (n=2 mice per group). (G) H&E and pCREB (green)/CK19 (red) co-I.F labeling with pCREB^{+} duct quantification in pancreata harvested from ctrl and ACP with recovery (n=6 mice per group). Scale bar, 50 µm. ^{ns}=nonsignificant; **p<0.01; ***, p<0.001; ****p<0.0001 by ANOVA.

Figure 2. ACP induction accelerates ADM reprogramming toward PanIN and pancreatic cancer in *Kras*$^{G12D/+}$ mutant mice. (A) Relative pancreas weight measurements in respective *KC* mice cohorts (n=5–7 mice per group). (B) Representative pancreatic images depicting H&E with quantification of CK19^{+} ducts, PanINs, collagen, and CD45^{+} in ctrl and ACP-induced *KC* mice with recovery periods (n=5 mice per group). (C) H&E staining within the pancreas depicting acinar, ADMs, PanINs, and cancer regions (n=3 mice per group). (D) UMAP projection displaying cell clusters and (E) cell count table, (F) volcano plot and (G) bubble plot within the acinar cells in the scRNA sequencing analysis of pancreata from ctrl and ACP-*KC* mice. (H) Representative pancreas images depicting amylase (green)/CK19 (red) co-I.F. (*top*) CK19^{+} amylase^{+} cell (*bottom*) quantification in ctrl and ACP-induced *KC* mice with 3- and 21-day recovery periods (n=3 mice per group). (I) qPCR analysis in the pancreas of ctrl and ACP-induced *KC* mice (n=3 mice per group). (J) Measurement of tumor latency period in ctrl, A, CP, and ACP-induced *KC* mice (n=12–13 mice per group). Scale bar, 50 µm. ^{ns}=nonsignificant; *p<0.05; **p<0.01; ****p<0.0001 by ANOVA or unpaired t-test.

Figure 3. Sustained hyperactivation of CREB in ACP *Kras*$^{G12D/+}$ driven ADM and PanIN progression. (A) H&E and co-I.F labeling of pCREB (green) and CK-19 (red) expression (*top*) with pCREB^{+} duct quantification within the ctrl and *KC* mice pancreata at 3- and 21-day ACP recovery period (*bottom*) (n=4 mice per group). (B) Western blotting of pCREB in pancreatic tissue lysates of control and *KC* mice at 3-, 21- and 42-day ACP recovery period (n=3 mice per group). (C) H&E images of the pancreas along with co-I.F labeling of pCREB (red)/CK19 (blue)/YFP (green), and YFP^{+} pCREB^{+} duct quantification in ctrl and *Ptf1a*$^{CreERTM/+}$; *LSL-Kras*$^{G12D/+}$; *R26R-EYFP* (*KCY*) mice at 3- and 21-day recovery periods (n=4 mice per group). (D) Schematic depicting sustained hyperactivation of CREB driving acinar cell neoplastic reprogramming in *KC* mice upon ACP induction. (E) IHC staining depicting pCREB expression within the pancreata of normal and CP tissues (*top*) of human CP and ACP patients with quantification (*bottom*). Scale bar, 50 µm. *p<0.05; **p<0.01; ***, p<0.001; ****p<0.0001 by ANOVA for three groups comparison and unpaired T-test for two groups.

Figure 4. Acinar-specific ablation of *Creb* attenuates spontaneous *Kras*$^{G12D/+}$ mediated PanIN progression. (A) Breeding strategy for generating acinar-specific *Creb* deficient *Kras** mutant mice (*Ptf1a*$^{CreERTM/+}$; *LSL-Kras*$^{G12D/+}$; *Creb*$^{fl/fl}$ or *KC*C$^{-/-}$). (B) Comparative measurement of relative pancreas weight in 10-month-old *Creb* wild type (*KC*) and *KC*C$^{-/-}$ mice (n=4–5 mice per group). (C) Representative photomicrographs of whole pancreas depicting significantly less tumor burden in *KC*C$^{-/-}$ mice than *KC* mice at 10 months of age. (D) Representative H&E images of the pancreata harvested from 5- and 10-month-old *KC* and *KCC*$^{-/-}$ mice. Scale bar, 10 and 50 µm. (E) Comparative assessment using H&E-based histology to examine the entire pancreas, illustrating acinar cells, ADMs, PanINs, and cancerous regions in 5- and 10-month-old *KC* and *KCC*$^{-/-}$ mice (n=3 mice per group). (F) Co-IF analysis of pCREB (green), CK-19 (red), and DAPI (blue) with quantification in pancreatic tissue sections harvested from 10-month-old *KC* and *KCC*$^{-/-}$ mice (n=4 mice per group). Scale bar, 50 µm. (G) Representative bright-field photomicrographs of primary 3D acinar cell cultures established from 10-month-old *KC* and *KCC*$^{-/-}$ mice (scale bar, 20 µm) (n=5 mice per group). (H) qPCR of pancreatic tissue harvested from *KC* and *KCC*$^{-/-}$ mice (n=3 mice per group). Scale bar, 10 and 50 µm. ^{ns}=nonsignificant; *p<0.05; **p<0.01; ***p<0.001; ****p<0.0001 one way ANOVA or unpaired t-test.

Figure 5. Acinar-specific ablation of *Creb* attenuates *Kras** induced progression of ADM/PanINs toward pancreatic cancer with ACP. (A) Comparative histological evaluation of mouse pancreas, accompanied by images showcasing H&E, CK-19, Alcian Blue, Sirius Red, and $CD45^+$ staining within *KC* and $KCC^{-/-}$ mice pancreata, ctrl and *KC* mice at 3- and 21-day ACP recovery period (n=5 mice per group). (B) H&E-based histological examination illustrating acinar cells, ADMs, PanINs, and cancerous regions in ctrl or within *KC* and $KCC^{-/-}$ mice pancreata harvested after 21 days of ACP recovery period (n=3 mice per group). (C) Pancreas images depicting amylase (green)/CK19 (red) and DAPI (blue) immunofluorescent labeling (*top*) and $CK19^+$ $amylase^+$ cell corresponding quantification (*bottom*) in ctrl (*KC* and $KCC^{-/-}$) or with ACP induction (n=3 mice per group). Scale bar, 50 µm. ^{ns}=nonsignificant; ****p<0.0001 by ANOVA.

Figure 6. Acinar-specific ablation of *Creb* attenuates ADM reprogramming and increases tumor latency period with ACP induction in *KC* mice. (A) Representative H&E images of the pancreas along with co-immunofluorescent labeling and YFP quantification (green)/CK19 (blue) in *Ptf1a-*$^{CreERTM/+}$*;LSL-Kras*$^{G12D/+}$*;R26R-EYFP (KCY)* and *Creb*$^{fl/fl}$ ($KCYC^{-/-}$) in control or with ACP induction (n=4 mice per group). (B) qPCR-based analysis of *KC* and $KCC^{-/-}$ mice pancreatic tissue with ACP induction (n=3 mice per group). (C) Tumor latency period assessment in ctrl or with ACP induction in *KC* and $KCC^{-/-}$ mice (n=12 mice per group, ctrl mice cohort represented here is similar to that shown in Figure 2*I*). (D) Schematic representation illustrating that acinar-specific *Creb* ablation diminishes pancreatic cancer progression in ACP induction in *KC* mice. *Translational relevance of CREB in PDAC with ACP*. (E) H&E and IHC staining depicting pCREB expression in patients with PDAC with chronic exposure to alcohol. (F) IHC staining of pCREB expression with quantification in human PDAC tumor vs. normal pancreas. (G) Therapeutic targeting of CREB using 666-15 (CREBi) in PDAC with ACP in an orthotopic KPC mouse model. Scale bar, 50 µm. ^{ns}=nonsignificant;*p<0.05; ****p<0.0001 by ANOVA or unpaired t-test.

Figure 7. (A) Schematic representation of ACP induction with *Kras** driving irreversible ADM reprogramming toward accelerated PDAC progression along with sustained CREB activation and increased fibroinflammation. (B and C) Acinar cell-specific deletion of CREB or

pharmacological inhibition of CREB using a targeted therapeutic approach generates profound anti-tumor responses and delays pancreatic cancer progression. The schematic was created with BioRender with License agreement numbers OW27SH91EN and WO27SH8QUH.

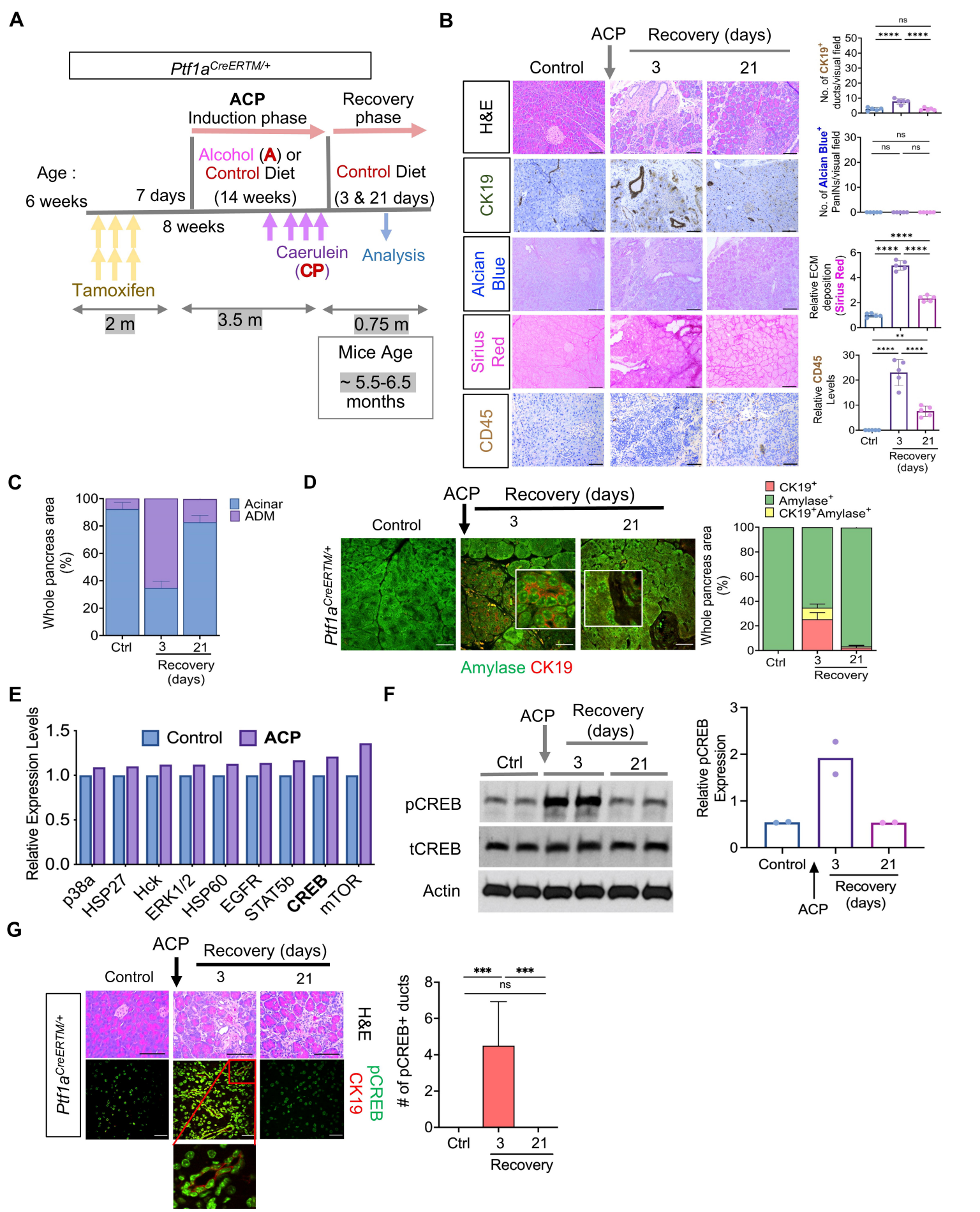
A
Ptf1a CreERTM/+
ACP
Induction phase
Recovery
phase
Alcohol (A) or
Control Diet
(14 weeks)
Control Diet
(3 & 21 days)
Age :
6 weeks
7 days
8 weeks
Caerulein
(CP)
Analysis
Tamoxifen
2 m
3.5 m
0.75 m
Mice Age
~ 5.5-6.5
months
B
ACP
Recovery (days)
Control
3
21
H&E
CK19
Alcian
Blue
Sirius
Red
CD45
No. of CK19+ ducts/visual field
No. of Alcian Blue+ PanINs/visual field
Relative ECM deposition (Sirius Red)
Relative CD45 Levels
Ctrl
Recovery
(days)
C
Whole pancreas area
(%)
Acinar
ADM
Ctrl
3
21
Recovery
(days)
D
ACP
Recovery (days)
Control
3
21
Ptf1a CreERTM/+
Amylase CK19
CK19+
Amylase+
CK19+Amylase+
Whole pancreas area
(%)
Ctrl
3
21
Recovery
E
Relative Expression Levels
Control
ACP
p38a
HSP27
Hck
ERK1/2
HSP60
EGFR
STAT5b
CREB
mTOR
F
ACP
Recovery
(days)
Ctrl
3
21
pCREB
tCREB
Actin
Relative pCREB
Expression
Control
3
21
Recovery
(days)
ACP
G
ACP
Recovery (days)
Control
3
21
Ptf1a CreERTM/+
H&E
pCREB
CK19
# of pCREB+ ducts
Ctrl
3
21
Recovery

Figure 1

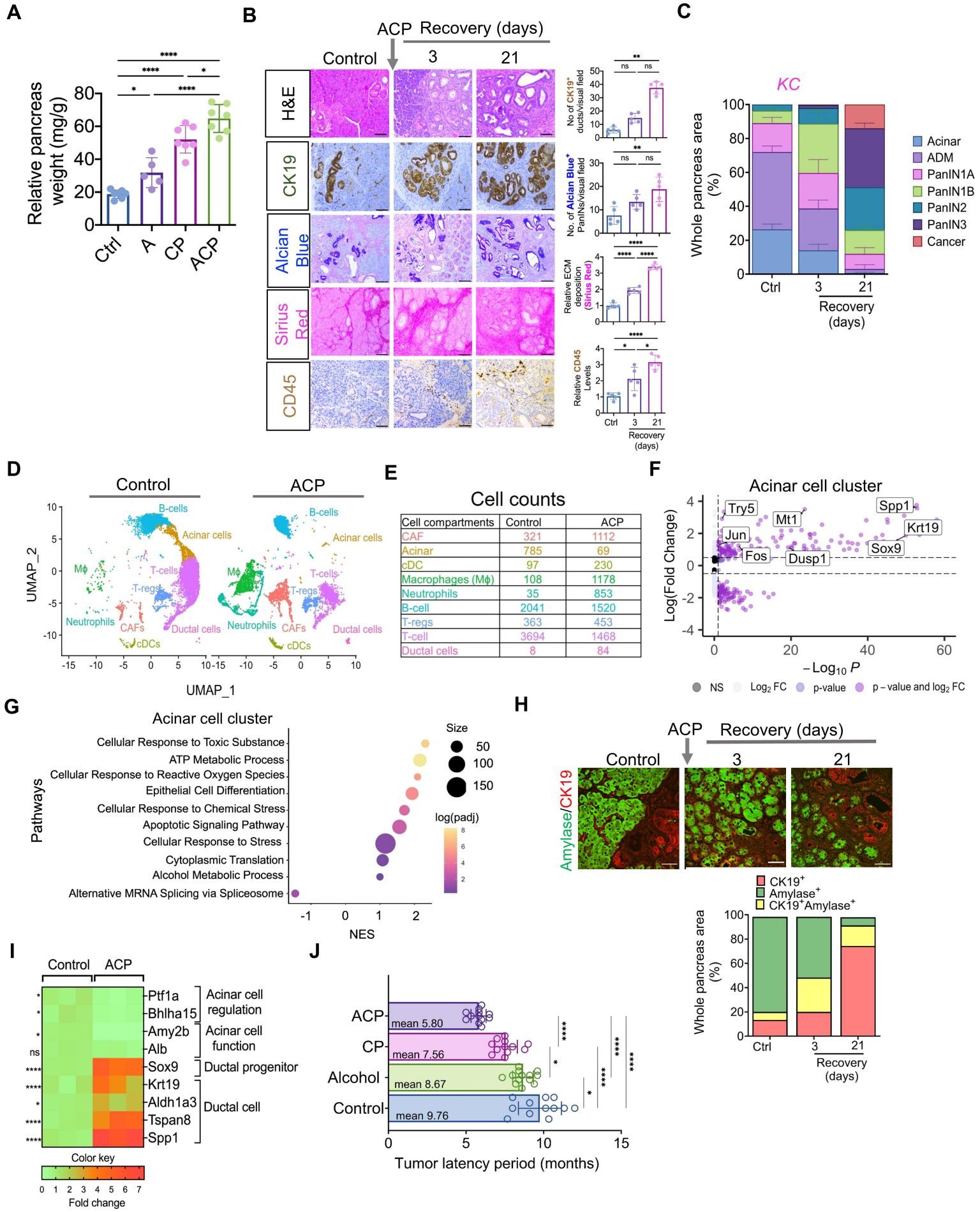
A
Relative pancreas weight (mg/g)
Ctrl
A
CP
ACP
B
ACP Recovery (days)
Control
3
21
H&E
CK19
Alcian Blue
Sirius Red
CD45
No. of CK19+ ducts/visual field
No. of Alcian Blue+ PanINs/visual field
Relative ECM deposition (Sirius Red)
Relative CD45 Levels
Recovery (days)
C
KC
Whole pancreas area (%)
Acinar
ADM
PanIN1A
PanIN1B
PanIN2
PanIN3
Cancer
Recovery (days)
D
Control
ACP
B-cells
Acinar cells
Mϕ
T-cells
T-regs
Neutrophils
CAFs
Ductal cells
cDCs
UMAP_2
UMAP_1
E
Cell counts
Cell compartments | Control | ACP
CAF | 321 | 1112
Acinar | 785 | 69
cDC | 97 | 230
Macrophages (Mϕ) | 108 | 1178
Neutrophils | 35 | 853
B-cell | 2041 | 1520
T-regs | 363 | 453
T-cell | 3694 | 1468
Ductal cells | 8 | 84
F
Acinar cell cluster
Try5
Mt1
Spp1
Krt19
Jun
Fos
Dusp1
Sox9
Log(Fold Change)
−Log10 P
NS
Log2 FC
p-value
p – value and log2 FC
G
Acinar cell cluster
Pathways
Cellular Response to Toxic Substance
ATP Metabolic Process
Cellular Response to Reactive Oxygen Species
Epithelial Cell Differentiation
Cellular Response to Chemical Stress
Apoptotic Signaling Pathway
Cellular Response to Stress
Cytoplasmic Translation
Alcohol Metabolic Process
Alternative MRNA Splicing via Spliceosome
Size
log(padj)
NES
H
ACP Recovery (days)
Control
3
21
Amylase/CK19
CK19+
Amylase+
CK19+Amylase+
Whole pancreas area (%)
Recovery (days)
I
Control
ACP
Ptf1a
Bhlha15
Amy2b
Alb
Sox9
Krt19
Aldh1a3
Tspan8
Spp1
Acinar cell regulation
Acinar cell function
Ductal progenitor
Ductal cell
Color key
Fold change
J
ACP
CP
Alcohol
Control
mean 5.80
mean 7.56
mean 8.67
mean 9.76
Tumor latency period (months)

Figure 2

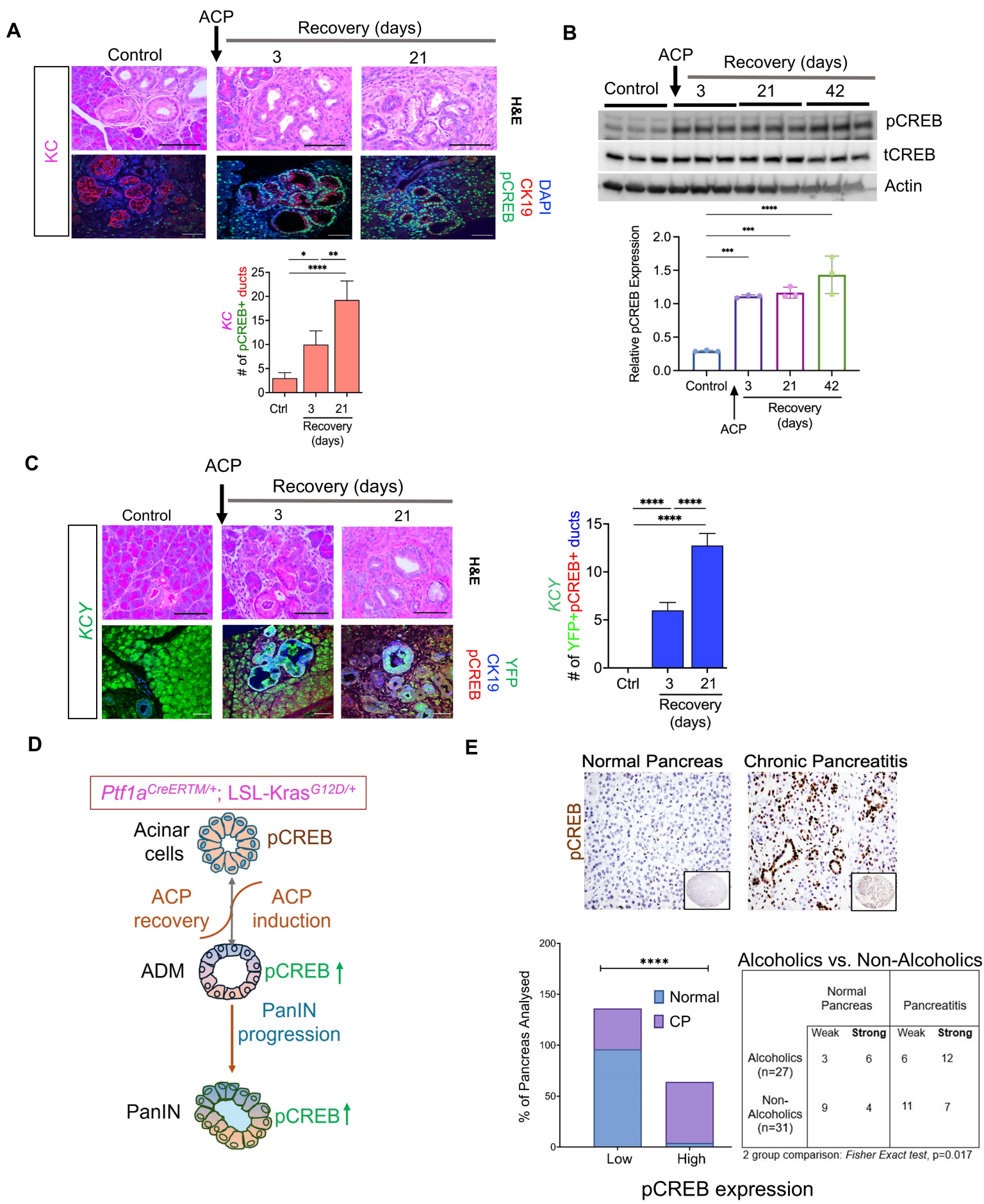
A
ACP
Recovery (days)
Control
3
21
KC
H&E
DAPI
CK19
pCREB
KC
# of pCREB+ ducts
Ctrl
Recovery (days)
B
ACP
Recovery (days)
Control
3
21
42
pCREB
tCREB
Actin
Relative pCREB Expression
Control
Recovery (days)
ACP
C
ACP
Recovery (days)
Control
3
21
KCY
H&E
YFP
CK19
pCREB
KCY
# of YFP+pCREB+ ducts
Ctrl
Recovery (days)
D
Ptf1aCreERTM/+; LSL-KrasG12D/+
Acinar cells
pCREB
ACP recovery
ACP induction
ADM
pCREB
PanIN progression
PanIN
pCREB
E
Normal Pancreas
Chronic Pancreatitis
pCREB
% of Pancreas Analysed
Normal
CP
Low
High
pCREB expression
Alcoholics vs. Non-Alcoholics
Normal Pancreas
Pancreatitis
Weak
Strong
Weak
Strong
Alcoholics (n=27)
3
6
6
12
Non-Alcoholics (n=31)
9
4
11
7
2 group comparison: Fisher Exact test, p=0.017

Figure 3

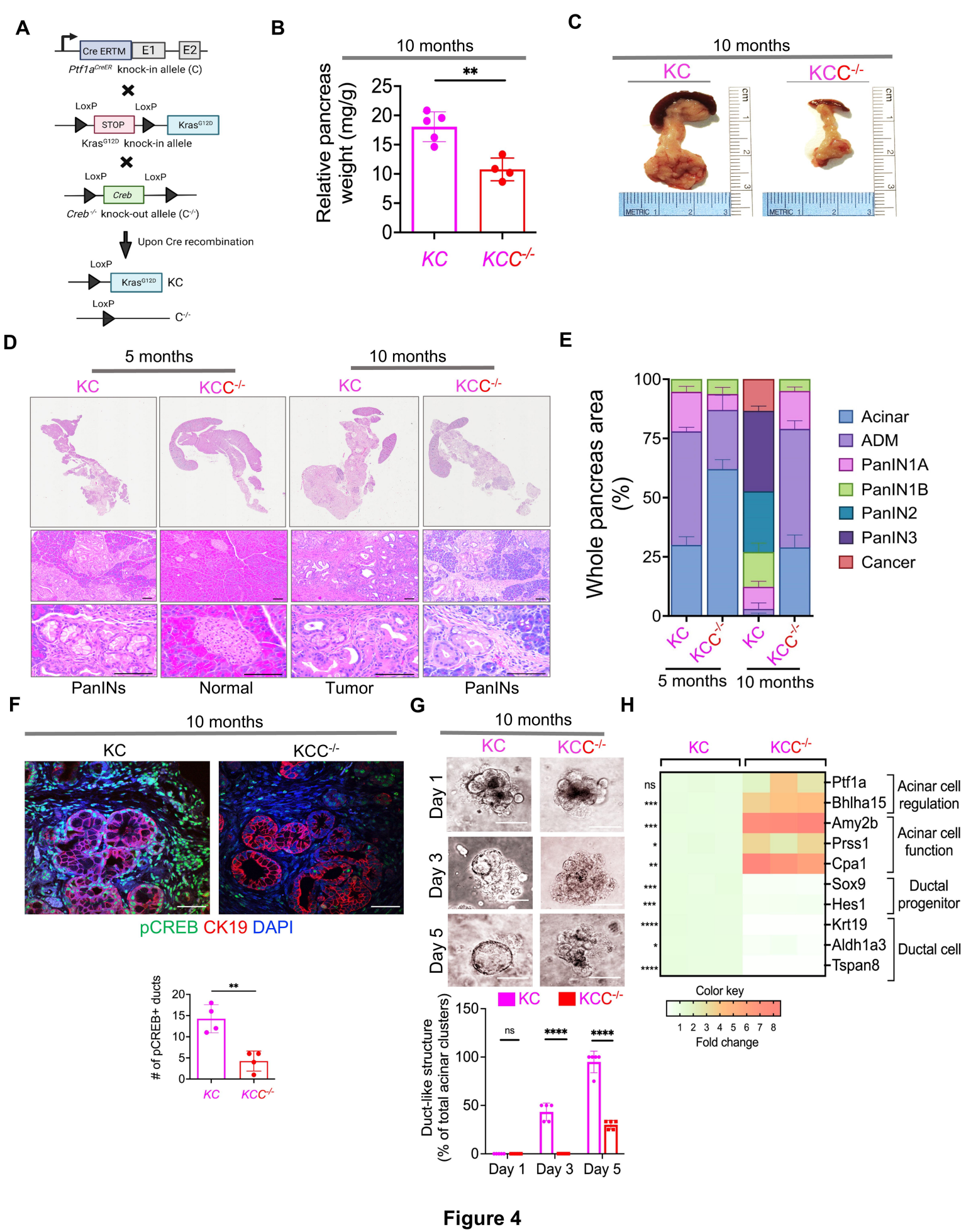
A
Cre ERTM
E1
E2
Ptf1a^CreER knock-in allele (C)
LoxP
STOP
Kras^G12D
Kras^G12D knock-in allele
Creb
Creb^-/- knock-out allele (C^-/-)
Upon Cre recombination
KC
C^-/-
B
10 months
Relative pancreas weight (mg/g)
**
KC
KCC^-/-
C
10 months
KC
KCC^-/-
D
5 months
10 months
PanINs
Normal
Tumor
PanINs
E
Whole pancreas area (%)
Acinar
ADM
PanIN1A
PanIN1B
PanIN2
PanIN3
Cancer
5 months
10 months
F
10 months
KC
KCC^-/-
pCREB CK19 DAPI
# of pCREB+ ducts
G
10 months
Day 1
Day 3
Day 5
Duct-like structure (% of total acinar clusters)
ns
****
H
Ptf1a
Bhlha15
Amy2b
Prss1
Cpa1
Sox9
Hes1
Krt19
Aldh1a3
Tspan8
Acinar cell regulation
Acinar cell function
Ductal progenitor
Ductal cell
Color key
Fold change

Figure 4

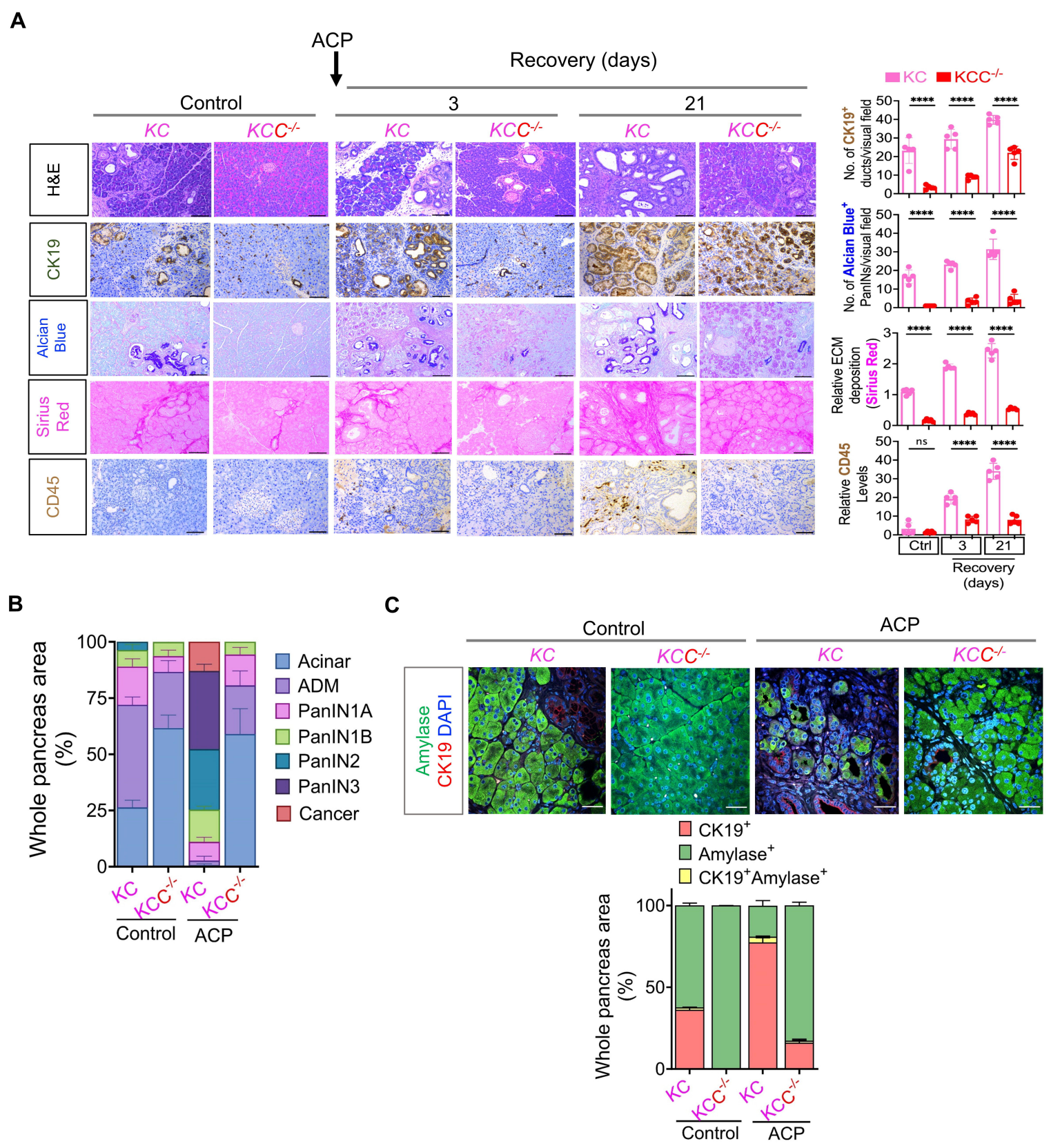
A
ACP
Recovery (days)
Control
3
21
KC
KCC-/-
H&E
CK19
Alcian Blue
Sirius Red
CD45
No. of CK19+ ducts/visual field
No. of Alcian Blue+ PanINs/visual field
Relative ECM deposition (Sirius Red)
Relative CD45 Levels
****
ns
Ctrl
Recovery (days)
B
Whole pancreas area (%)
Acinar
ADM
PanIN1A
PanIN1B
PanIN2
PanIN3
Cancer
C
Amylase CK19 DAPI
CK19+
Amylase+
CK19+Amylase+

Figure 5

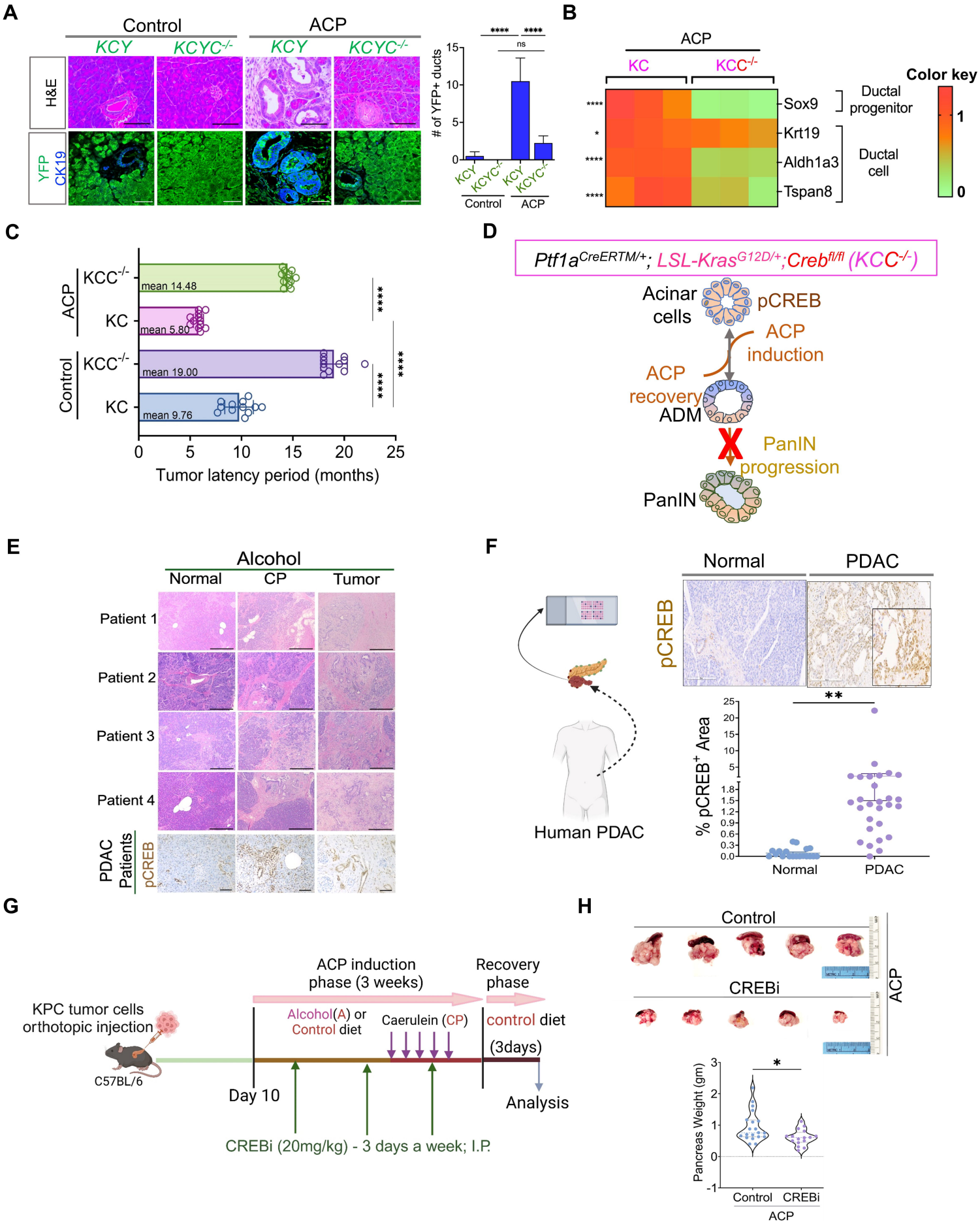
A
Control
ACP
KCY
KCYC-/-
KCY
KCYC-/-
H&E
YFP
CK19
# of YFP+ ducts
****
****
ns
Control
ACP
B
ACP
KC
KCC-/-
Sox9
Krt19
Aldh1a3
Tspan8
Ductal progenitor
Ductal cell
Color key
1
0
C
ACP
Control
KCC-/-
KC
mean 14.48
mean 5.80
mean 19.00
mean 9.76
Tumor latency period (months)
D
Ptf1aCreERTM/+; LSL-KrasG12D/+;Crebfl/fl (KCC-/-)
Acinar cells
pCREB
ACP induction
ACP recovery
ADM
PanIN progression
PanIN
E
Alcohol
Normal
CP
Tumor
Patient 1
Patient 2
Patient 3
Patient 4
PDAC Patients
pCREB
F
Normal
PDAC
pCREB
Human PDAC
% pCREB+ Area
**
Normal
PDAC
G
KPC tumor cells orthotopic injection
C57BL/6
ACP induction phase (3 weeks)
Recovery phase
Alcohol(A) or Control diet
Caerulein (CP)
control diet (3days)
Day 10
Analysis
CREBi (20mg/kg) - 3 days a week; I.P.
H
Control
CREBi
ACP
Pancreas Weight (gm)
*
Control
CREBi
ACP

Figure 6

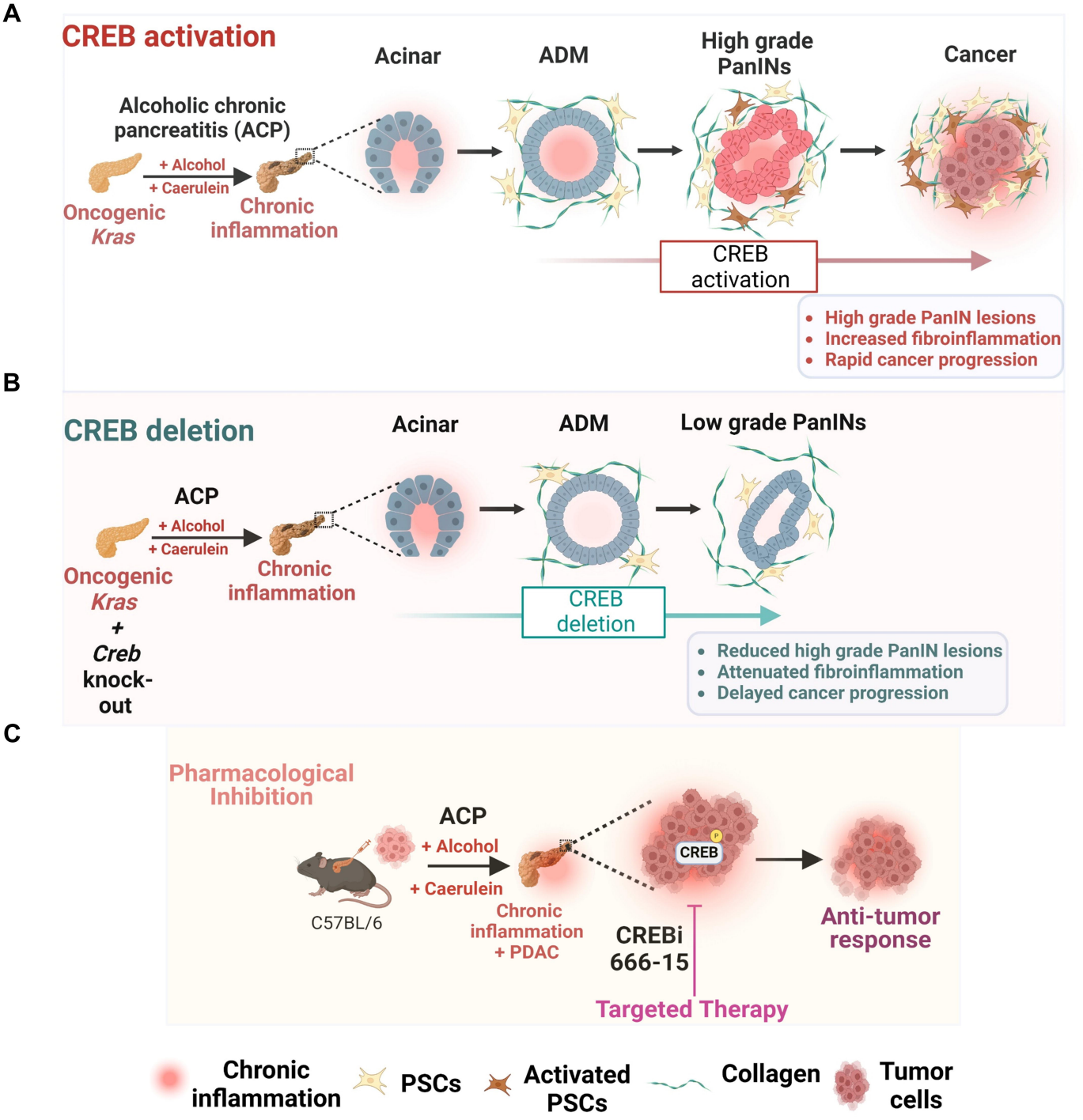
A
CREB activation
Acinar
ADM
High grade PanINs
Cancer
Alcoholic chronic pancreatitis (ACP)
+ Alcohol
+ Caerulein
Oncogenic Kras
Chronic inflammation
CREB activation
High grade PanIN lesions
Increased fibroinflammation
Rapid cancer progression
B
CREB deletion
Acinar
ADM
Low grade PanINs
ACP
+ Alcohol
+ Caerulein
Oncogenic Kras + Creb knock-out
Chronic inflammation
CREB deletion
Reduced high grade PanIN lesions
Attenuated fibroinflammation
Delayed cancer progression
C
Pharmacological Inhibition
ACP
+ Alcohol
+ Caerulein
C57BL/6
Chronic inflammation + PDAC
CREB
CREBi 666-15
Targeted Therapy
Anti-tumor response
Chronic inflammation
PSCs
Activated PSCs
Collagen
Tumor cells

Figure 7